Dynamic Stability and THD Reduction Governing of an Integrated Grid-Connected Offshore Wind Farm and Marine-Current Farm Using FACTS (STATCOM)

Vangapalli Kiran Kumar
B.Tech,
Dept of EEE,
Mahatma Gandhi Institute of Technology, Hyderabad.

Mosam Abhilesh
B.Tech,
Dept of EEE,
Mahatma Gandhi Institute of Technology, Hyderabad.

Indoori Srivani
B.Tech,
Dept of EEE,
Mahatma Gandhi Institute of Technology, Hyderabad.

ABSTRACT:

This paper presents a control scheme and total harmonic distortion (THD) reduction based on a static synchronous compensator (STATCOM) to achieve both voltage control and damping enhancement of a grid-connected integrated 80-MW offshore wind far m (OWF) and 40-MW marine-current farm (MCF). The performance of the studied OWF is simulated by an equivalent doubly-fed induction generator (DFIG) driven by an equivalent wind turbine (WT) while an equivalent squirrel-cage rotor induction generator (SCIG) driven by an equivalent marine current turbine (MCT) is employed to simulate the characteristics of the MCF.

A damping controller of the STATCOM is designed by using modal control theory to contribute effective damping characteristics to the studied system under different operating conditions. A frequency-domain approach based on a linearized system model using Eigen value techniques and a time-domain scheme based on a nonlinear system model subject to various disturbances are both employed to simulate the effectiveness of the proposed control scheme.It can be concluded from the simulated results that the proposed STATCOM joined with the designed damping controller is very effective to stabilize the studied system under disturbance conditions.

TECHNOLOGIES USED:

- Static synchronous compensator.
- Static synchronous compensator.
- Doubly-fed induction generator.
- Squirrel-cage rotor induction generator.
- Total harmonic distortion.
- Dynamic stability.
- Marine-current farm.
- Offshore wind farm.

INTRODUCTION:

Ocean energy may include thermal energy, wave energy, offshore wind energy, tidal energy, ocean current energy, etc. Generators driven by marine-current turbine (MCT) combined with offshore generators driven by wind turbine (WT) will become a novel scheme for energy production in the future.

Since oceans cover more than 70% surface of the earth, a hybrid power generation system containing both offshore wind farm (OWF) and marine-current farm (MCF) can be extensively developed at the specific locations of the world in the future.

Block diagram:
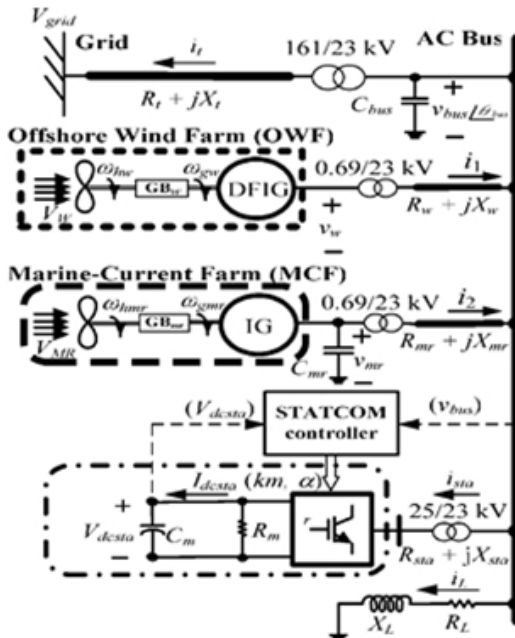
Configuration of the integrated OWF and MCF with STATCOM

To run an MCF may use several squirrel-cage induction generators (SCIGs) connected directly to the power grid through an offshore step-up transformer and undersea cables. Both WTs and MCTs have very similar operating characteristics but an SCIG-based MCF requires reactive power for magnetization while a DFIG-based OWF with two bidirectional power converters can control its output power factor to be close to unity. When the generated active power of an SCIG-based MCF is varied due to marine-current fluctuations, the absorbed reactive power and the terminal voltage of the MCF can be significantly affected.A large-scale OWF may combine with different FACTS devices or energy-storage systems for example STATCOM etc.

PROSED SYSTEM:

The analyzed results of stability improvement of power systems using STATCOMs and the damping controller design of STATCOMs.

The design of an output feedback linear quadratic controller for a STATCOM and a variable-blade pitch of a wind energy conversion system to perform both voltage control and mechanical power control under grid-connection or islanding conditions. System modeling and controller design for fast load voltage regulation and mitigation of voltage flicker using a STATCOM.A new D- STATCOM control algorithm enabling separate control of positive- and negative-sequence currents was proposed, and the algorithm was based on the developed mathematical model in the coordinates for a D-STATCOM operating under unbalanced conditions. An in-depth investigation of the dynamic performance of a STATCOM and a static synchronous series compensator (SSSC) using digital simulations.

The results of a study on the application of the recently developed STATCOM for the damping of torsion oscillations occurred in a series compensated AC system were studied while dynamic performance of the nonlinear system with an optimized STATCOM controller was evaluated under a three-phase fault condition.Discussion and comparison of different control techniques such as PSS, static VAR compensator (SVC) and STATCOM for damping undesirable inter area oscillations in power systems.The conventional method of PI control for a STATCOM was compared and contrasted with various feedback control strategies, and a linear optimal control based on LQR control was shown to be superior in terms of response profile and control effort required.

MODELS OF THE STUDIED INTEGRATED OWF AND MCF:

A. Wind Turbine
B. Mass-Spring-Damper System and Induction Generator.
C. Power Converters of DFIG
D. Marine-Current Speed and Marine-Current Turbine

Wind Turbine:

The mechanical power (in W) produced by a WT can be expressed by

$$P_{mw} = \frac{1}{2} \rho_\omega \cdot A_{rw} \cdot V_W^3 \cdot C_{PW}(\lambda_\omega, \beta_\omega) \qquad (1)$$

Where :

ρω is the air density in kg/m
Arw is the blade impact area,
m VW is the wind speed in m/s, and
CPW is the power coefficient of theWT.

The wind speed VW is modeled as the algebraic sum of a base wind speed, a gust wind speed, a ramp wind speed, and a noise wind speed.

B. Mass-Spring-Damper System and Induction Generator
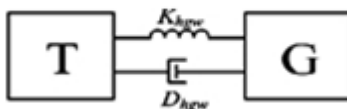
Two-inertia reduced-order equivalent mass-spring-damper model of the WT coupled to the rotor shaft of the studied wind DFIG.

Above figure shows the two-inertia reduced-order equivalent massspring-damper model of the WT coupled to the rotor shaft of the studied wind DFIG. The effect of the equivalent gearbox (GBω) between the WT and the DFIG has been included in this model.
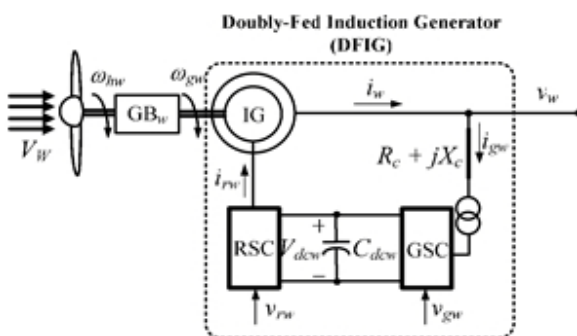
One-line diagram of the studied doubly-fed induction generator.

The per-unit q - and d -axis voltage-current equations of an induction generator and they can be used for the electrical parts of the wind DFIG and the marine-current SCIG.

C. Power Converters of DFIG:

For normal operation of a wind DFIG, the input AC-side volt- ages of the RSC and the GSC can be effectively controlled to achieve the aims of simultaneous output active-power and reactive-power control.Below shows the control block diagram of the RSC of the studied DFIG. As shown inbelow figure, the operation of the RSC requires *idrw*and *iqrw*to follow the varying reference points that are determined by maintaining the output active power and the stator-winding voltage at the setting values, respectively. The required voltage for the RSC is (*vrw*) derived.
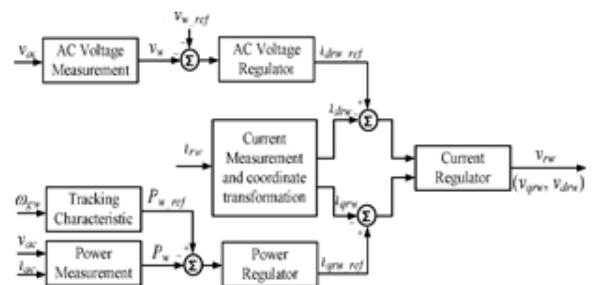
Control block diagram for the RSC of the DFIG.

D. Marine-Current Speed and Marine-Current Turbine
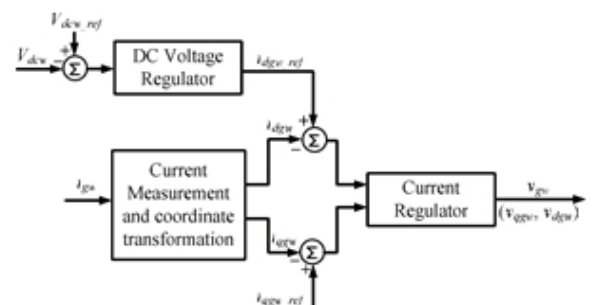
Control block diagram for the GSC of the DFIG.

The MCT is assumed to be driven by tide velocities, and the current velocity is determined by spring and neap tides.

The marine-current speeds are given at hourly intervals starting at 6 h before high waters and ending 6 h after. It is easy to derive a simple and practical model for marine current speed under the knowing tide coefficients as follows:

$$V_{MR} = V_{nt} + \frac{(C_{mr} - 45)(V_{st} - V_{nt})}{95 - 45} \qquad (2)$$

Where:

Cmr is the marine coefficient, 95 and 45 are the spring and neap tide medium coefficients, respectively, and Vst and Vnt are the spring and neap marine-current speeds, respectively. The employed marine-current model is between France to England area. The mechanical power (in W) generated by the studied MCT can be expressed by

$$P_{mmr} = \frac{1}{2} \rho_{mr} \bullet A_{rmr} \bullet V^3_{MR} \bullet C_{pmr}(\lambda_{mr}, \beta_{mr}) \qquad (3)$$

Where:

ρ mr is the seawater density in kg/ 3 m (1025 ρ mr = kg/ 3 m), Armr is the blade impact area in 2 m , VMR is the marine velocity in m/s as depicted in (2), and Cpmr is the power coefficient of the MCT. The cut-in, rated, and cut-out speeds of the studied MCT are 1, 2.5, and 4 m/s, respectively. When VMR is higher than the rated speed, the pitch-angle control system of the MCT activates to limit the output power of the MCT at the rated value.
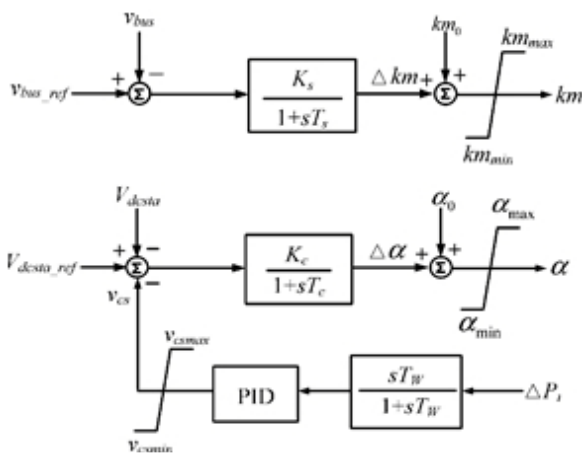
Control block diagram of the proposed STATCOM including the designed PID damping controller.

TABLE I
Employed System Parameters

System bases
V_{base} = 690 V, S_{base} = 2 MW, ω_{base} = $2\pi f_{base}$, f_{base} = 60 Hz
Single WT-DFIG of the studied 80-MW OWF
r_{sw} = 0.00706 pu, X_{sw} = 0.171 pu, r_{rw} = 0.005 pu
X_{rw} = 0.156 pu, X_{mw} = 2.9 pu, C_{dcw} = 1.0 pu
H_{gw} = 0.5 pu, H_{tw} = 2.5 pu, K_{hgw} = 0.3 pu, D_{hgw} = 0.05 pu
K_{Pw} = 10.2, K_{Iw} = 30.0, τ_w = 100 s, $\beta_{w\ min}$ = 0°, $\beta_{w\ max}$ = 30°
Single MCT-SCIG of the studied 40-MW MCF
r_{smr} = 0.00488 pu, X_{smr} = 0.09241 pu, r_{rmr} = 0.00549 pu
X_{rmr} = 0.09955 pu, X_{mmr} = 3.95279 pu
H_{gmr} = 0.5 pu, H_{tmr} = 3.5 pu, K_{hgmr} = 0.1 pu, D_{hgmr} = 0.1 pu
K_{Pmr} = 20.0, K_{Imr} = 30.0, τ_{mr} = 120 s, $\beta_{mr\ min}$ = 0°, $\beta_{mr\ max}$ = 30°
STATCOM (±32 MVAR)
R_m = 500 pu, C_m = 0.074 F
R_{sta} = 0.05 pu, X_{sta} = 0.2 pu, T_s = 0.01 s, K_s = 0.1
T_c = 0.01 s, K_c = 0.5, km_{max} = 1.0, km_{min} = 0.0, km_0 = 0.5
α_{max} = 45°, α_{min} = -45°, α_0 = 0°, v_{csmax} = 0.2, v_{csmin} = -0.2
Transmission lines, capacitor banks, and local load
R_w = 0.02 pu, X_w = 0.4 pu
R_{mr} = 0.02 pu, X_{mr} = 0.4 pu, C_{mr} = 0.3125 pu
R_l = 0.04 pu, X_l = 0.8 pu, C_{bus} = 0.125 pu, R_L = 8.0 pu, X_L = 4.0 pu
Constants of power coefficients of WT and MCT
c_1 = 0.34, c_2 =128, c_3 = 0.4, c_4 = c_5 = 0, c_6 = 11
c_7 = 10.9, c_8 = 0.08, c_9 = 0.01
d_1 = 0.18, d_2 =85, d_3 = 0.38, d_4 = 0.25, d_5 = 0.5, d_6 = 10.2
d_7 = 6.2, d_8 = 0.025, d_9 = -0.0443

TABLE II
EIGENVALUES (RAD/S) [DAMPING RATIOS] OF THE STUDIED SYSTEM UNDER WIND SPEED OF 12 M/S AND MARINE-CURRENT SPEED OF 2.5 M/S

		OWF + MCF	OWF + MCF + STATCOM	OWF + MCF + STATCOM + PID
$\Lambda_{1,2}$	X_{DFIG}	-7.12 ± j371.14 [0.01918]	-6.99 ± j371.15 [0.01883]	-7.06 ± j371.14 [0.01902]
$\Lambda_{3,4}$		-5.03 ± j37.29 [0.13368]	-5.09 ± j37.882 [0.13316]	-5.42 ± j37.109 [0.14452]
$\Lambda_{5,6}$	X_{SCIG}	-21.26 ± j373.74 [0.05679]	-21.25 ± j373.74 [0.05677]	-21.34 ± j373.75 [0.05700]
$\Lambda_{7,8}$		-114.05 ± j16.128 [0.99015]	-125.11 ± j2.9282 [0.99972]	-125.2 ± j10.96 [0.99619]
$\Lambda_{9,10}$		-3.41 ± j4.8212 [0.57745]	-5.41 ± j4.7722 [0.74993]	-5.5 ± j4.8* [0.75342]
$\Lambda_{11,12}$		-13.64 ± j0.6579 [0.99883]	-15.44 ± j0.5579 [0.99934]	-15.5 ± j0.56* [0.99935]
$\Lambda_{13,14}$	X_{MECH}	-1.52 ± j5.1231 [0.28444]	-1.46 ± j5.6831 [0.24882]	-1.47 ± j5.1231 [0.27581]
$\Lambda_{15,16}$		-6.62, -4.01	-6.61, -4.03	-6.62, -4.01
$\Lambda_{17,18}$		-2.03, -2.84	-2.01, -2.82	-2.13, -3.1
$\Lambda_{19,20}$		-20.55 ± j3988.77 [0.005152]	-37.55 ± j4435.3 [0.008466]	-37.41 ± j4435.5 [0.008434]
$\Lambda_{21,22}$	X_{ELEC}	-733.53 ± j376.77 [0.88952]	-736.13 ± j377.68 [0.88973]	-736.05 ± j377.64 [0.88973]
$\Lambda_{23,24}$		-16.11 + j376.22 [0.04278]	-16.11 ± j376.22 [0.04278]	-16.06 + j376.15 [0.04249]
$\Lambda_{25,26}$		-	-89.64 ± j789.42 [0.11283]	-92.77 ± j788.2 [0.11689]
$\Lambda_{27,28}$	X_{STA}	-	-122.66 ± j215.55 [0.49458]	-118.81 ± j218.75 [0.47727]
Λ_{29}		-	-91.05	-92.22

*denotes exactly assigned eigenvalues

The eigenvaluesΛ −Λ 9 18 andΛ −Λ 19 24 listed in Table II refer to the mechanical modes and the electrical modes of the studied system, respectively.

The eigenvalues$\Lambda - \Lambda$ 25 29 refer to the modes of the STATCOM. An examination of the eigenvalues listed in Table II has the following points.

1) The DFIG modes, the SCIG modes, and the electrical modes of the studied system are almost fixed on the complex plane;

2) The damping of both $\Lambda 9,10$ and$\Lambda 11,12$ is slightly improved when the STATCOM is connected to the integrated OWF and MCF. The damping of both$\Lambda 9,10$ and$\Lambda 11,12$ can be simultaneously improved by the addition of the designed PID damping controller;

3) All system eigenvalues are located on the left half of the complex plane under a fixed wind speed and a fixed marine-current speed.

The control block diagram of the phase angle α of the STATCOM including the PID damping controller was shown in above figure. It is seen that the PID damping controller employs the active-power deviation of the transmission line (ΔPt) as a feedback signal to generate a damping signal vcs in order that the damping characteristics of the poorly damped modes $\Lambda 9,10$ and$\Lambda 11,12$ listed in Table II can be effectively improved.Hence, the output signal in (9)
 isY P $= \Delta$ t andU v $=$ cs is the input vector. The transfer function H(s) of the proposed PID damping controller in domain is given by

$$H(s) = \frac{U(s)}{Y(s)} = \frac{v_{cs}(s)}{\Delta P_t(s)}$$
$$= \frac{sT_W}{1+sT_W}\left(K_P + \frac{K_I}{s} + sK_D\right) \qquad (10)$$

Where:

TW is the time constant of the wash-out term while KP , KI , and KD are the proportional, integral, and derivative gains of the damping controller, respectively. Taking the Laplace transformation, an algebraic equation of the closed-loop system containing the PID damping controller can be obtained.

The input signal in domain can be expressed by

$$U(s) = H(s)\Delta P_t(s) = H(s)Y(s) = H(s)CX(s). \qquad (11)$$

Combining (10)-(11), we have

$$sX(s) = \{A + B[H(s)C]\}X(s). \qquad (12)$$

The characteristic equation of the closed-loop system including the PID damping controller is given by

$$\det\{sI - [A + BH(s)C]\} = 0. \qquad (13)$$

Pre specified Eigenvalues:

$$\Lambda_{9,10} = -5.5 \pm j4.8 \quad \Lambda_{11,12} = -15.5 \pm j0.56.$$

Parameters of the Designed PID Damping Controller:

$$K_P = 10.5, K_I = 2.37, K_D = 0.06, T_W = 0.08s.$$

The system eigen values of the studied integrated OWF and MCF with the proposed STATCOM joined with the designed PID damping controller are listed in the fifth column of Table II. It can be clearly observed that both $\Lambda 9,10$ and $\Lambda 11,12$ have been exactly positioned on the desired locations on the complex plane. Some major constraints for selecting the assigned eigenvalues are simply depicted as below.

1) The obtained parameters of the PID damping controller should be. For example, the time constant of the washout term must be positive and the gains of the PID damping controller should be as small as possible.

2) The eigenvalues of the closed-loop system including the designed PID damping controller should be completely located on the left half of the complex plane at the selected operating conditions. According to the eigenvalue results listed in the fifth column of Table II and the four parameters of the designed PID damping controller of the STATCOM shown above, it can be concluded that both constraints 1) and 2) mentioned above can be simultaneously met.

STEADY-STATE ANALYSIS UNDER VARIOUS OPERATING CONDITIONS

This section presents the steady-state operating condition results of the studied system when VW is increased from 4 to 24 m/s while VMR is increased from 1 to 4 m/s. below graph shows the 3-D plots for the calculated steady-state operating conditions of the studied system under the selected values for VW and VMR The steady-state operating conditions shown in below figure are analyzed as below.
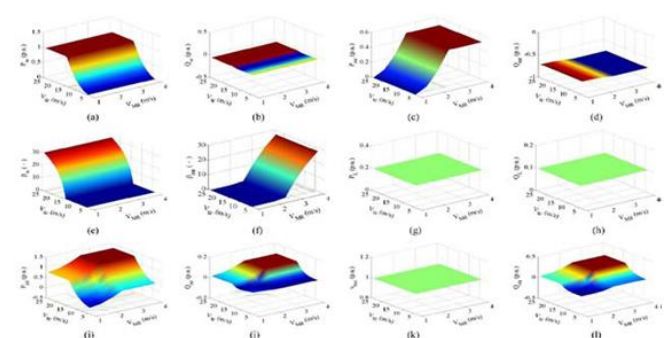
Steady-state operating conditions of the studied system under various values of wind speed and marine-current speed (a) Pw , (b) Qw , (c) Pmr , (d) Qmr , (e) β w , (f) β mr , (g) PL , (h) QL , (i) Pgrid , (j)Qgrid , (k) bus v , (l) Qsta .

NONLINEAR MODEL SIMULATIONS:

By compare the damping characteristics contributed by the proposed STATCOM joined with the designed PID damping controller on dynamic stability improvement of the studied system under a noise wind speed disturbance, a marine-current speed disturbance, and a three-phase shortcircuit fault at the grid, respectively.
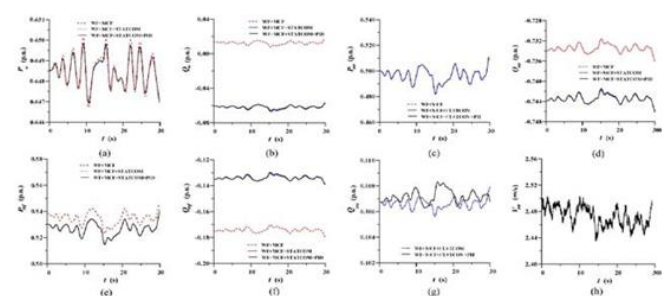
Dynamic responses of the studied system with and without the designed PID STATCOM damping

controller under a noise wind speed disturbance (a) Pw , (b) Qw , (c) Pmr , (d) Qmr , (e) Pgrid , (f) Qgrid , (g) bus v , (h) VW
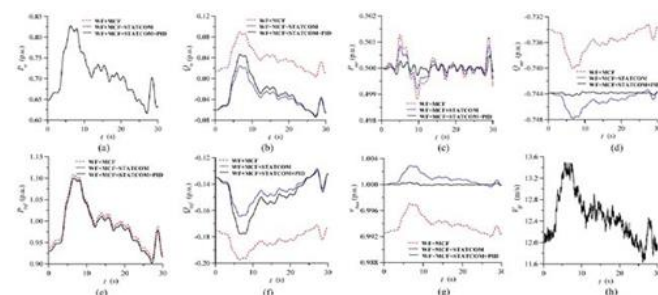
Dynamic responses of the studied system with and without the PID STATCOM damping controller under a marine- current speed disturbance (a) Pw , (b) Qw , (c) Pmr , (d) Qmr , (e) Pgrid , (f)Qgrid , (g) Qsta , (h)VM

A. Noise Wind-Speed Disturbance:

Above figure of with PID controller (a)-(g) illustrates the studied system with and without the proposed STATCOM and the designed PID damping controller under the noise wind-speed disturbance shown in Above figure of with PID controller (h). The simulation sequence is as below:

When 0 0.5 st s << , the OWF operates under a base wind speed of 12 m/s and the MCF operates under a base marine-current speed of 2.5 m/s;

When 0.5 30 st s << , the noisewind speed shown in Above figure of with PID controller (h) is added to the system but the marine-current speed is still kept atVMR =2.5 m/s. The dynamic simulation results shown in Above figure of with PID controller (a)-(g) are analyzed as below.

The amplitudes of the active power delivered to the power grid P grid shown in figure of with PID controller 10(e) and the active power generated by the SCIG of the MCF shown in figure of with PID controller(c) can be slightly reduced and the absorbed reactive power from the power grid Qgrid shown in

figure of with PID controller (f) can be decreased when the STATCOM joined with the PID controller is included in the studied system.The generated active power of the DFIG Pw shown in figure of with PID controller (a) is not affected by the addition of the STATCOM with the PID controller.

B. Marine-Current Speed Disturbance:

Above figure without PID controller (a)-(g) plots the studied system with and without the proposed STATCOM and the designed PID damping controller under the marine-current speed disturbance shown in without PID controller(h). When t s < 0 , the OWF operates under a base wind speed of VW = m/s and the MCF operates under a base marine current speed of 2.5 VMR = m/s. It is seen from the dynamic simulation results shown in Fig.11(a)-(g) that all quantities are slightly deviated from the steady-state operating points at t s = 0 due to the small variations on marine-current speed.Above figure shows without PID

C. Three-Phase Short-Circuit Fault at Power Grid:

Below graphs plots the transient responses of the studied system with and without the proposed STATCOM joined with the designed PID damping controller under a three-phase short-circuit fault at the grid. The OWF operates under a base wind speed of 12 m/s while the MCF operates under a base marine-current speed of 2.5 m/s. A three phase short-circuit fault is suddenly applied to the grid at t s =1 and is cleared at t s =1.2 .

It is seen from the transient simulation results shown in below plots that most quantities suddenly drop to low values when the fault occurs. When the fault is cleared, all responses shown in below plots. 12 stably return the original steady-state operating conditions within 4 s. The proposed STATCOM with the designed PID damping controller can offer better damping characteristics to the studied system under the severe

three phase short-circuit fault than without the PID controller.
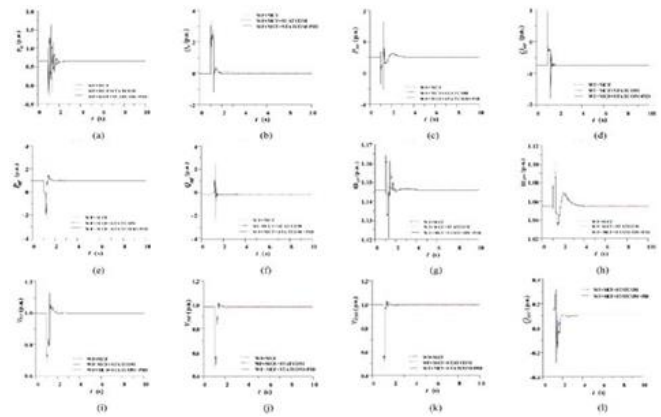
Transient responses of the studied system with and without the designed PID STATCOM damping controller under a three-phase fault at power grid (a) Pw , (b) Qw , (c) Pmr , (d) Qmr , (e) Pgrid , (f) Qgrid , (g) ωrω, (h) ωrmr , (i) VW , (j) VMR , (k) bus v , (l) Qsta

CONCLUSION:

This paper has presented the dynamic stability improvement and total harmonic distortion reduction of an integrated OWF and MCF using a STATCOM. A PID damping controller has been designed for the STATCOM by using a unified approach based on pole-assignment approach. Eigenvalue calculations and time-domain simulations of the studied system subject to a noise wind-speed disturbance, a marine-current speed disturbance, and a three-phase shortcircuit fault at the grid have been systematically performed to demonstrate the effectiveness of the proposed STATCOM joined with the designed PID damping controller on suppressing voltage fluctuation of the studied system and improving system dynamic stability under different operating conditions.

REFERENCES:

[1] K. R. Padiyar and N. Prabhu, "Design and performance evaluation of subsynchronous damping controller with STATCOM," IEEE Trans. Power Del., vol. 21, no. 3, pp. 1398-1405, Jul. 2006.

[2] W. L. Chen and Y. Y. Hsu, "Controller design for an induction generator driven by a variable-speed wind turbine," IEEE Trans. EnergyConvers., vol. 21, no. 3, pp. 635-625, Sep. 2006.

[3] A. Jain, K. Joshi, A. Behal, and N. Mohan, "Voltage regulation with STATCOMs: Modeling, control and results," IEEE Trans. Power Del.,vol. 21, no. 2, pp. 726- 735, Apr. 2006.

[4] B. Blăzic and I. Papic, "Improved D-STATCOM control for operation with unbalanced currents and voltages," IEEE Trans. Power Del., vol. 21, no. 1, pp. 225-233, Jan. 2006.

[5] A. H. Norouzi and A. M. Sharaf, "Two control schemes to enhance the dynamic performance of the STATCOM and SSSC," IEEE Trans. Power Del., vol. 20, no. 1, pp. 435-442, Jan. 2005.